CHEMISTRY OF MATERIALS

ARTICLE

pubs.acs.org/cm

Photodeposition of Co-Based Oxygen Evolution Catalysts on α-Fe_2O_3 Photoanodes

Kenneth J. McDonald and Kyoung-Shin Choi*

Department of Chemistry, Purdue University, West Lafayette, Indiana 47907, United States

Supporting Information

ABSTRACT: Cobalt-based oxygen evolution catalysts containing phosphates (Co-Pi OEC) were photochemically deposited onto the surface of n-type α-Fe_2O_3 electrodes to enhance solar O_2 production. α-Fe_2O_3 films used in this study were prepared by electrodepositing Fe films followed by thermal oxidation at 500 °C. The use of a nonaqueous plating solution made it possible to deposit adherent and uniform Fe films, which is difficult to achieve in an aqueous medium. Photodeposition of Co-Pi OEC was carried out by using photogenerated holes in the valence band of α-Fe_2O_3 to oxidize Co^{2+} ions to Co^{3+} ions in a phosphate buffer solution, which resulted in the precipitation of Co-Pi OEC on the α-Fe_2O_3 surface. Two different deposition conditions, open circuit (OC) and short circuit (SC) conditions, were studied comparatively to understand their effect on the growth and composition of Co-Pi OEC deposits. The results showed that the SC condition where the photoreduction reaction is physically separated from the photo-oxidation reaction significantly increased the yield and nucleation density of Co-Pi OECs, resulting in a better coverage of the α-Fe_2O_3 surface with Co-Pi OEC nanoparticles. X-ray photoelectron spectroscopy showed that the OC condition resulted in a higher Co^{2+}/Co^{3+} ratio in the Co-Pi OEC deposits than the SC condition. This difference in composition is due to the simultaneous photoreduction occurring on the α-Fe_2O_3 surface under OC conditions. Co-Pi OEC improved the photocurrent of α-Fe_2O_3 electrodes more than Co^{2+} ions simply adsorbed on the α-Fe_2O_3 surface and the Co-Pi OEC deposited under SC conditions resulted in the most pronounced photocurrent enhancement. These results demonstrate the advantages of creating a SC condition for photodeposition of Co-Pi OECs. O_2 detection measurements show that the presence of photodeposited Co-Pi OEC on the α-Fe_2O_3 surface not only increases the total amount of photocurrent generated by facilitating electron−hole pair separation but also increases the photocurrent to O_2 conversion efficiency by improving O_2 evolution kinetics.

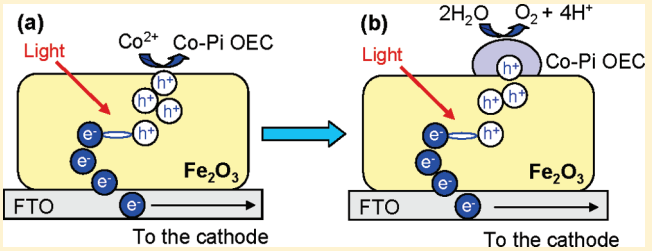

KEYWORDS: iron oxide, photoelectrochemical cell, photoelectrolysis, oxygen evolution catalyst, photodeposition

INTRODUCTION

α-Fe_2O_3 is an n-type semiconductor with many desirable properties for use as a photoanode in a water-splitting photoelectrochemial cell. It has a band gap of 2.1 eV which allows for utilizing a significant visible portion of the solar spectrum and a valence band position with sufficient overpotential for oxidizing water to O_2. Furthermore, it is environmentally benign, very abundant, and capable of withstanding neutral and alkaline conditions. However, for use as a photoanode for water oxidation, α-Fe_2O_3 suffers from poor charge transport properties and slow interfacial kinetics for water oxidation.[1−3] Many strategies have been developed to overcome these challenges, which include tuning compositions (e.g., doping),[3−9] construction of nanostructured electrodes,[3,10−14]and addition of O_2 evolution catalysts.[3,15−17]

Recently, Nocera and co-workers reported a simple anodic electrodeposition route to produce an oxygen-evolving catalyst (Co-Pi OEC) using an aqueous neutral phosphate medium containing Co^{2+} ions.[18−22] The deposition mechanism involves the oxidation of Co^{2+} ions to Co^{3+} ions which have limited solubility at pH 7 causing the precipitation of amorphous cobalt-based oxide/hydroxide deposits containing phosphates. In order to use this catalyst not for electrolysis of water but for photoelectrolysis of water, the Co-Pi OEC needs to be coupled with an n-type semiconductor (photoanode).[16,17,23] Gamelin and co-workers have demonstrated that electrodeposited Co-Pi OEC on an α-Fe_2O_3 photoanode indeed enhanced the photocurrent and O_2 evolution.[16,17]

We have recently demonstrated that the Co-Pi OEC can also be produced by photodeposition on the surface of an n-type semiconductor without the need of an electrical bias, using ZnO as an example.[23] In this method, photogenerated holes in the valence band of ZnO were used to oxidize Co^{2+} ions to Co^{3+} ions. Because the redox potential of the Co^{2+}/Co^{3+} couple is similar to that of H_2O/O_2, any n-type semiconductor that has a proper valence band position to evolve O_2 can ideally also oxidize

Received: July 24, 2010
Revised: February 6, 2011
Published: March 10, 2011

Scheme 1. (a) Schematic Diagram Showing the Band Positions of α-Fe_2O_3 and the Redox Potentials of Co^{2+}/Co^{3+} ($[Co^{2+}]$ = 0.5 mM) and H_2O/O_2 in a pH 7 Aqueous Medium; Schematic Representation for (b) Photodeposition of Co-Pi OEC and (c) Photo-oxidation of Water on an n-type α-Fe_2O_3 Electrode; Both Reactions Consume Photo-generated Holes

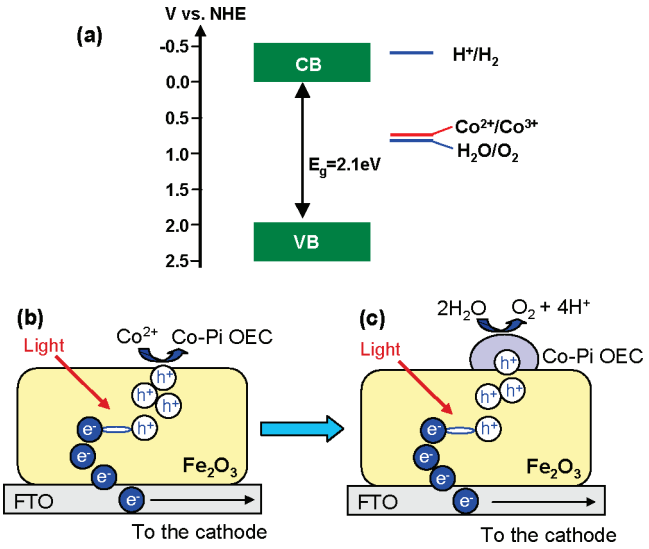

Co^{2+} ions to photodeposit Co-Pi OECs (Scheme 1a).[23,24] The distinctive advantage of coupling Co-Pi OEC with a photoanode via photodeposition is that when photodeposited, Co-Pi OEC is deposited where photogenerated holes are the most readily available (Scheme 1b). Since solar O_2 evolution is also a photo-oxidation reaction consuming photogenerated holes, photodeposition of Co-Pi OEC has the effect of placing Co-Pi OECs on the most active sites on the semiconductor surface for solar O_2 evolution (Scheme 1c). This self-site-selective photodeposition of Co-Pi OECs makes the most effective use of Co-Pi OECs and, therefore, enhances O_2 evolution with a minimal amount of Co-Pi OEC.

In this study, we report the photodeposition of Co-Pi OECs onto the surface of n-type α-Fe_2O_3 electrodes. In particular, we studied two different photodeposition conditions, short-circuit (SC) and open-circuit (OC) conditions, and examined how these conditions affect the yield, growth, and composition of Co-Pi OEC deposits on the α-Fe_2O_3 electrodes. The α-Fe_2O_3 electrodes used in this study are prepared by electrodeposition of iron metal films followed by thermal oxidation treatment. The synthesis, characterization, and photoelectrochemical properties of α-Fe_2O_3 and α-Fe_2O_3/Co-Pi OEC electrodes are investigated in detail.

EXPERIMENTAL SECTION

Synthesis of α-Fe_2O_3. Iron films were electrodeposited by reduction of Fe^{2+} ions using a dimethyl sulfoxide (DMSO) (Mallinckrodt) solution containing 0.05 M $Fe(ClO_4)_2 \cdot xH_2O$ (Aldrich). The solution was purged with argon to prevent the reduction of O_2 during the depositions that can compete with the reduction of Fe^{2+} ions and lower deposition efficiency. The deposition was carried out potentiostatically at 110 °C using a VMP2Multichannel Potentiostat (Princeton Applied Research). A standard three-electrode setup in an undivided cell was used. The electrodes used were fluorine-doped tin oxide (FTO) (8−12 Ω resistance) as the working electrode, a glass slide sputter coated with 1000 Å of platinum on 300 Å of titanium as the counter electrode, and an Ag/AgCl electrode in 4 M KCl as the reference electrode against which all potential mentioned hereafter were measured. Prior to use FTO substrates were cleaned by soaking and stirring in a 2 wt % Alconox solution at 95 °C for 5 min followed by sonicating and thoroughly rinsing with copious amount of isopropyl alcohol and water.

After exploring various conditions, the optimum deposition potential of E = −1.4 V (average deposition current density of ∼5.67 mA/cm^2) was found to produce uniformly black transparent films. Increasing deposition potential or temperature resulted in films with poor adhesion. Decreasing the potential below −1.2 V or the temperature below 95 °C resulted in a significant decrease in deposition rate. After deposition, the as deposited films were rinsed thoroughly with deionized water, and dried with a gentle stream of nitrogen gas. To obtain crystalline α-Fe_2O_3 electrodes, we annealed as deposited films in atmosphere at 500 °C for 1 h (ramping rate = 2 °C/min).

Photodeposition of Co-Pi OECs. For photodeposition of Co-Pi OECs under OC condition, an α-Fe_2O_3 electrode was immersed in a Petri dish containing 0.5 mM cobalt chloride and 0.1 M potassium phosphate at pH 7. Photodepositions were performed using a hand-held UV light (UVM-57, λ = 302 nm) with an output voltage of 1.5 μW/cm^2. For photodeposition of Co-Pi OECs under SC condition, a counter electrode, which was 1000 Å of platinum deposited on 300 Å of titanium on a glass slide by sputter coating, was also immersed in the same solution and short circuited to the α-Fe_2O_3 electrode. For the OC condition both photo-oxidation and photoreduction occur on the same α-Fe_2O_3 surface, but for SC condition, only photo-oxidation occurs on the α-Fe_2O_3 surface and photoreduction occurs on the counter electrode. In a given solution, the photogenerated holes and electrons are expected to be used mainly for oxidation of Co^{2+} to Co^{3+} and reduction of dissolved O_2, respectively. The optimum deposition times of Co-Pi OECs under OC and SC conditions were 30 and 10 min, respectively, which were determined by the photocurrent enhancement of the resulting α-Fe_2O_3/Co-Pi OEC electrodes. After depositions, samples were rinsed thoroughly with deionized water, and dried with a gentle stream of nitrogen gas.

Electrodeposition of Co-Pi OEC on FTO. Using electrodeposition conditions reported by Kanan and Nocera, Co-Pi OEC was deposited on FTO by applying +1.2 V against Ag/AgCl in an electrolyte containing 0.5 mM $CoCl_2$ and 0.1 M potassium phosphate buffer (pH 7).[18] After deposition, samples were rinsed thoroughly with deionized water, and dried with a gentle stream of nitrogen gas.

α-Fe_2O_3 with Adsorbed Co^{2+}. α-Fe_2O_3 samples were soaked in a solution containing a 0.5 mM cobalt chloride and 0.1 M potassium phosphate at pH 7 for 30 min in the dark.[18] After soaking, samples were rinsed thoroughly with deionized water and dried with a gentle stream of nitrogen gas.

Characterization. X-ray diffraction (XRD) patterns were collected using a Scintag X2 diffractometer (Cu K_α radiation). Scanning electron microscopy (SEM) images were taken using a field emission scanning electron microscope (FEI Nova NanoSEM) operated at 5 kV. All films were coated with Pt using a thermal evaporator before imaging to minimize charging problems. UV−vis spectra of the films were measured using a Cary 300 UV−vis spectrophotometer in dual-beam transmittance, with bare FTO substrate as a reference. X-ray Photoelectron Spectroscopy (XPS) data were obtained by a Kratos Ultra DLD spectrometer using monochromatic Al K_α radiation (1486.58 eV). The spectra were collected at an angle normal to the substrate, and the atomic concentrations of the chemical elements in the near-surface region were estimated after the subtraction of a Shirley type background, taking into account the corresponding Scofield atomic sensitivity factors and inelastic mean free pass (IMFP) of photoelectrons as a standard procedure of CasaXPS software. All spectra were calibrated to C_{1s} = 284.6 eV.

dx.doi.org/10.1021/cm1020614 |*Chem. Mater.* 2011, 23, 1686–1693

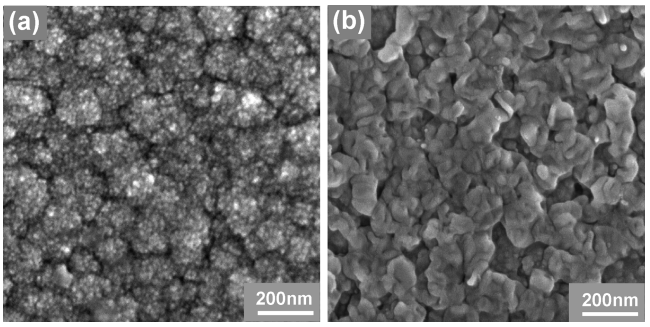

Figure 1. SEM images of (a) as-deposited (Fe) and (b) annealed (α-Fe_2O_3) films.

Photocurrent Measurements. Photoelectrochemical performance of α-Fe_2O_3 and α-Fe_2O_3/catalyst electrodes was tested using a 300 W Xe arc lamp (Oriel) with light illuminated through fiber optics with the output power of 100 mW/cm^2 with an AM 1.5G filter and a spot size of 0.20 cm^2 aimed at the α-Fe_2O_3/electrolyte interface (front illumination). The electrolyte was either 1 M NaOH solution (pH~13.6) or 1 M NaOH solution containing 0.1 M KH_2PO_4 bubbled with Ar gas prior to photocurrent measurements in order to purge the dissolved oxygen. The counter electrode was an oversized platinum prepared the same as previously mentioned and the reference was a Ag/AgCl in 4 M KCl. For linear sweep voltammetry (LSV) with chopped illumination (chopping frequency = 0.33 Hz), potential was swept from +0.65 to −1 V at 5 mV/s.

Dark Scans. Onset of electrochemical O_2 evolution for α-Fe_2O_3 and catalyst modified α-Fe_2O_3 electrodes was measured using LSV in the dark. All electrodes were masked with Teflon tape to expose an identical geometrical area (0.28 cm^2) for measurement. The electrolyte was 1 M NaOH solution bubbled with Ar gas prior to photocurrent measurements in order to purge the dissolved oxygen. Counter and reference electrode were as described previously. For LSV, the potential was swept from −0.1 V to +0.65 V at 10 mV/s.

Oxygen Detection. Oxygen was detected quantitatively using an Ocean Optics fluorescence-based oxygen sensor (FOSPOR-R 1/16"). The electrochemical cell was a custom-built airtight two-compartment cell divided by a frit. One side held a Pt counter electrode, while the other side held the working electrode (α-Fe_2O_3 or α-Fe_2O_3 /Co-Pi OEC) along with a Ag/AgCl reference electrode. Both sides were filled with 1 M NaOH containing 0.1 M KH_2PO_4 and the electrolyte and the headspace of the sealed cell were purged with argon. The electrolyte in the working compartment was 30.0 mL and the headspace volume was 11.75 mL. The needle probe was inserted through a rubber septum for O_2 readings throughout the experiment. The probe was calibrated using 2 points (argon, 0% O_2, and air, 20.9% O_2), with an error of 5% of the reading. The experiment began with 30 min of baseline O_2 measurement followed by 4 h of illumination using light passed through an AM 1.5 filter and adjusted to 600 mW/cm^2 (6 Suns) and 0.2 V applied bias. The use of an intense light (600 mW/cm^2) for the O_2 detection experiment was to ensure a higher signal-to-noise ratio and therefore more reliable data. The probe measures the O_2 content in the headspace and records as mole %. This was converted to μmol after first adjusting for the O_2 dissolved in solution using Henry's Law. The charge passed during the experiment was also converted from Coulombs to μmols by dividing by 4 F and multiplying by 10^6 (F = 96 485 C/mol).

RESULTS AND DISCUSSION

The α-Fe_2O_3 electrodes used in this study were prepared by cathodic deposition of nanocrystalline Fe films using a nonaqueous solvent, DMSO. Deposition of Fe films using an aqueous medium usually results in poor quality films because typical deposition conditions for Fe films result in simultaneous H_2 evolution.[25−28] The use of a nonaqueous medium eliminated this problem and enabled the deposition of uniform and well-adherent nanoparticulate Fe films as shown in Figure 1a. The Fe films were converted to n-type α-Fe_2O_3 electrodes by annealing in air at 500 °C for 1 h. The color of the films changed from black to transparent orange after the thermal oxidation process. The bandgap of the α-Fe_2O_3 electrode was estimated to be *ca.* 2.1 eV by the UV−vis absorption spectrum (see the Supporting Information, Figure S1), which is in a good agreement with previous studies of α-Fe_2O_3. An SEM image of the α-Fe_2O_3 electrode shows that the thermal oxidation process smoothened the surface morphology (Figure 1b). The purity and crystallinity of the Fe and α-Fe_2O_3 films were confirmed by X-ray diffraction (JCPDS 06−0696 for Fe metal and JCPDS 33−0664 for α-Fe_2O_3) (see the Supporting Information, Figure S2).

Co-Pi OEC was photodeposited on α-Fe_2O_3 electrodes using two different deposition conditions, open circuit (OC) and short circuit (SC) conditions (Scheme 2). Under the OC condition, both the photo-oxidation and photoreduction reactions occur on the α-Fe_2O_3 surface. Under the SC condition, the photogenerated majority charge carriers (electrons for n-type α-Fe_2O_3) move to the counter electrode to be consumed, thus separating the photoreduction reaction from the photo-oxidation reaction occurring on the α-Fe_2O_3 surface. The SC condition may have the advantage of decreasing electron−hole recombination and increasing the efficiency of the photodeposition reaction. However, no comparative studies on photodeposition on the

Scheme 2. Schematic Representation Showing Where Photo-Oxidation and Photo-reduction Reactions Occur under (A) Open Circuit (OC) and (b) Short Circuit (SC) Conditions When an n-Type α-Fe_2O_3 Electrode Is Illuminated

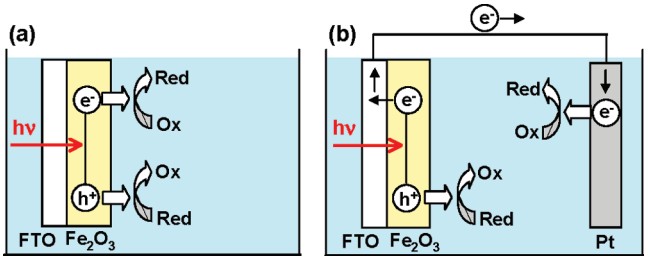

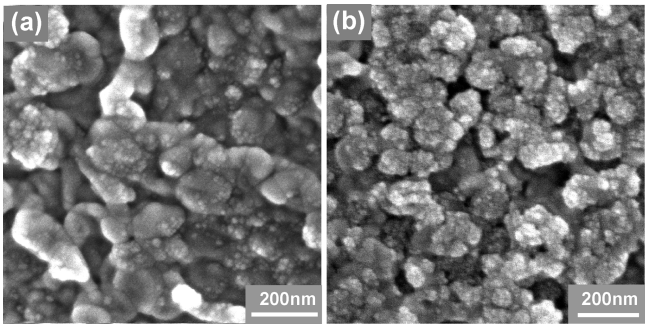

Figure 2. SEM images of Co-Pi OECs deposited on the α-Fe_2O_3 surface using (a) OC condition for 30 min and (b) SC condition for 10 min.

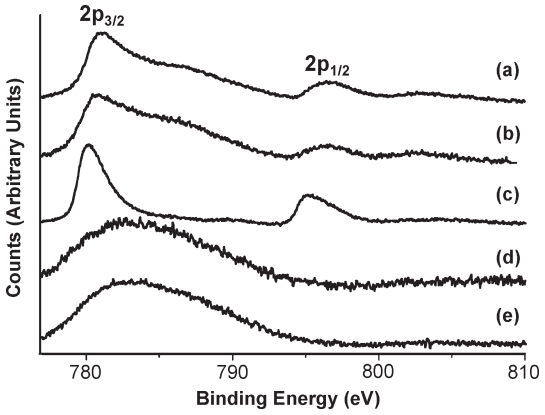

Figure 3. Co 2p XPS of (a) Co-Pi OEC (OC) on α-Fe_2O_3, (b) Co-Pi OEC (SC) on α-Fe_2O_3, and (c) electrodeposited Co-Pi OEC on FTO. XPS of (d) bare α-Fe_2O_3 and (e) Co^{2+} adsorbed on α-Fe_2O_3 showing the Fe L_3VV Auger peak that falls on the Co $2p_{3/2}$ region.

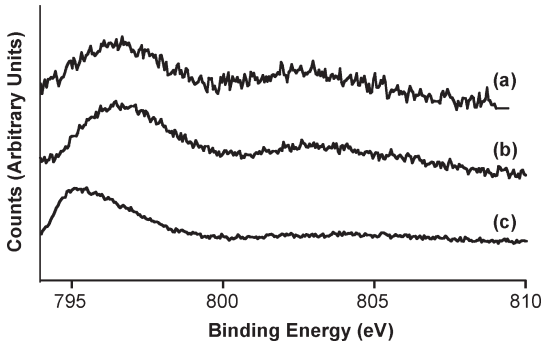

Figure 4. Co $2p_{1/2}$ XPS of (a) Co-Pi OEC (OC) on α-Fe_2O_3, (b) Co-Pi OEC (SC) on α-Fe_2O_3, and (c) electrodeposited Co-Pi OEC on FTO.

semiconductor surface using both OC and SC conditions have been previously reported.

Figure 2 shows SEM images of Co-Pi OECs deposited under OC condition for 30 min and under SC condition for 10 min (Figure 2a, b). In these images, nanoparticulate Co-Pi OEC deposits can be easily recognized against the smooth surface of the α-Fe_2O_3 electrode. The time selected for each condition was optimized to maximize photocurrent of the resulting α-Fe_2O_3/Co-Pi OEC electrodes. Shorter or longer deposition than the optimum duration for each condition resulted in a decrease in photocurrent due to either insufficient OEC coverage on the Fe_2O_3 surface or the presence of excess OEC which reduces the photon absorption by the Fe_2O_3 electrode. The SEM images show that creating a SC condition increased not only the total yield of Co-Pi OEC but also the nucleation density significantly, resulting in a better coverage of the α-Fe_2O_3 surface although the deposition time was only 1/3 of the duration used for the OC condition. Due to the enhanced nucleation density, the size of each Co-Pi OEC particle in the sample prepared under SC condition was kept smaller. Increasing the surface coverage without growing large OEC particles is advantageous because catalytic enhancement can be achieved while minimizing the interference of OEC with light absorption by the α-Fe_2O_3 electrodes.

To investigate whether the OC and SC conditions also affected the oxidation states of Co ions in the Co-Pi OEC deposits, an XPS study was carried out. Co-Pi OEC electrodeposited on an FTO substrate as well as on an α-Fe_2O_3 film containing surface adsorbed Co^{2+} ions, which was prepared by simply dipping the α-Fe_2O_3 film in the same solution used for photodeposition, were also examined for comparison. The Co^{2+} ions adsorbed on the α-Fe_2O_3 surface were reported to exhibit catalytic activity for water oxidation.[3] Because photodeposition of Co-Pi OECs on the surface of α-Fe_2O_3, which involves immersing an α-Fe_2O_3 electrode in a Co^{2+}-containing solution, may also result in simple adsorption of Co^{2+} ions on the surface, XPS and other characterizations of Co^{2+}-adsorbed α-Fe_2O_3 electrodes are necessary to distinguish the effect of Co-Pi OECs from that of surface adsorbed Co^{2+} ions.

Figure 3a-c shows that the cobalt 2p XPS peaks of photodeposited Co-Pi OECs using both OC and SC conditions are much broader than that of the Co-Pi OEC electrodeposited on an FTO substrate. The broad feature in the Co $2p_{3/2}$ region (780−794 eV) of the photodeposited Co-Pi OECs on α-Fe_2O_3 is due to the Fe L_3VV Auger peak that falls in this reagion,[29,30] which was confirmed by examining the same region of the XPS spectrum of the bare α-Fe_2O_3 electrode (Figure 3d). The Co $2p_{3/2}$ peak of the photodeposited Co-Pi OECs, which look comparable to the Co $2p_{3/2}$ peak of the electrodeposited Co-Pi OEC, could be obtained when the contribution from the Fe L_3VV Auger peak was subtracted by curve fitting (see the Supporting Information, Figure S3). The Co 2p spectrum of Co^{2+} ions adsorbed on the α-Fe_2O_3 surface (Figure 3e) looked almost identical to the Fe L_3VV Auger peak obtained from the bare α-Fe_2O_3 electrode (Figure 3d), suggesting that the signal generated by the surface adsorbed Co^{2+} ions is not substantial and cannot be easily distinguished from the Fe L_3VV Auger peak when Al K_a radiation is used.

More useful information regarding the presence of Co^{2+}/Co^{3+} ions in the Co-Pi OECs was obtained by analyzing the position and intensity of the Co $2p_{1/2}$ peak that appears in the 794−808 eV region where no interference from the Fe Auger peak is present (Figure 3d). Figure 4 shows that the main Co $2p_{1/2}$ peaks of the photodeposited Co-Pi OECs are significantly shifted to a higher energy compared to that of electrodeposited Co-Pi OEC which appears at *ca.* 795 eV. The main Co $2p_{1/2}$ peak of Co^{3+} ions typically appears between 794.0 and 794.7 eV, and the shift of this peak to a higher binding energy is indicative of an increase in the Co^{2+}/Co^{3+} ratio in the sample.[31−33] Therefore, our result indicates that the photodeposited Co-Pi OECs contain more Co^{2+} ions than electrodeposited Co-Pi OEC in general. (A recent electron paramagnetic resonance (EPR) study reported that electrodeposited Co-Pi OEC contains high spin Co^{2+}.)[34]

Another difference found among the Co $2p_{1/2}$ peaks shown in Figure 4 is the intensity of the Co $2p_{1/2}$ satellite peaks that appear at *ca.* 802.5 eV, which progressively increase from electrodeposited Co-Pi OEC, to Co-Pi OEC (SC), and to Co-Pi-OEC (OC). Increased intensity of the satellite peak with respect to the main $2p_{1/2}$ peak is related to the Co^{2+} (high spin)/Co^{3+} ratio.[31−33,35] Therefore, the difference in the intensity of the Co $2p_{1/2}$ satellite peaks also supports the conclusion that the photodeposited Co-Pi OECs on the α-Fe_2O_3 surface contain more Co^{2+} ions than electrodeposited Co-Pi OECs and that the OC condition results in a higher Co^{2+}/Co^{3+} ratio in the Co-Pi OEC than the SC condition.

Co-Pi OEC (OC) contains more Co^{2+} ions probably because a portion of the photoexcited electrons in the conduction band of the α-Fe_2O_3 are likely used to reduce Co^{3+} ions in the Co-Pi

OEC to Co^{2+} ions under the OC condition. This is equivalent to the surface recombination of electrons and holes, because some photogenerated holes will be used to reoxidize the Co^{2+} ions in the OEC back to Co^{3+} ions instead of oxidizing Co^{2+} ions in solution to form new Co-Pi OEC deposits. This explains why the nucleation density and the catalyst loading obtained under the OC condition are lower than those obtained under the SC condition. The fact that the Co-Pi OEC (SC) contains less Co^{2+} ions than its OC counterpart but more than electrodeposited Co-Pi OEC suggests that even under the SC condition not all the photoexcited electrons are transferred to the counter electrode. Instead, a fraction of them appears to leak to the surface of α-Fe_2O_3 where they are used to reduce Co^{3+} ions in the Co-Pi OEC. Back reduction of the photo-oxidation product by electrons at the surface of α-Fe_2O_3 electrodes has been observed previously in other photoelectrochemical cells.[36,37]

We believe that the Co^{2+}/Co^{3+} ratio in the as-deposited Co-Pi OECs is not as important as the total amount or nucleation density of the Co-Pi OECs in affecting the overall catalytic ability, because the oxidation states of Co ions in the catalyst are supposed to continuously change in a cyclic manner ($Co^{2+} \rightarrow Co^{3+}/Co^{4+} \rightarrow Co^{2+}$) during the course of water oxidation.[19,35] However, the detailed XPS study on the oxidation states of Co ions in the as-prepared OEC provided critical information to understand and confirm the difference between the OC and SC conditions used in the photodeposition of Co-Pi OECs.

The Co:P ratio in the Co-Pi OECs was estimated by integrating the P 2p and Co 2p XPS spectra. Both Co-Pi OECs (OC and SC) show that the Co:P ratio is 1:0.9−1. This ratio deviates from the 2:1 Co:P ratio of the electrochemically prepared thick Co-Pi OEC layer and suggest that the photodeposited Co-Pi OEC nanoparticles contain more phosphate ions as in the case of the previously reported nanoparticulate Co-Pi OECs photodeposited on ZnO.[18,23]It has been recently reported that while the presence of phosphates at the catalyst/electrolyte interface is important for the optimum performance of Co-Pi OECs,[20−22,38] phosphates do not participate in the construction of the core Co-catalytic centers in a stoichiometric manner. Instead the oxygen atoms of phosphates appear to serve as the termination groups of the Co clusters. Therefore, the Co:P ratio is expected to depend on the size of the Co-Pi OEC clusters or the surface area to volume ratio of the Co-Pi OECs particles. This explains why the Co:P ratios of the photodeposited nanoparticulate Co-Pi OECs are smaller than that obtained from a few micrometers thick Co-Pi OEC layer prepared electrochemically.

The effect of photodeposited Co-Pi OECs on the photocurrent of α-Fe_2O_3 electrodes was investigated by measuring I−V characteristics with chopped light, which generates both the dark current and the photocurrent during a single linear sweep (Figure 5a). The I−V characteristics of a Co^{2+}-adsorbed α-Fe_2O_3 electrode were also obtained for comparison. The expanded plot in Figure 5(b) shows that anodic photocurrent of the bare α-Fe_2O_3 electrode gradually decreases as the potential is swept to the negative direction and is converted to cathodic photocurrent at −0.4 V vs Ag/AgCl. The conversion of n-type behavior to p-type behavior can be observed at the flatband potential of a semiconductor electrode that is very lightly doped.[1] All other α-Fe_2O_3 electrodes containing Co-Pi OECs or adsorbed Co^{2+} ions show the same conversion of n-type behavior to p-type behavior near −0.4 V, indicating that the deposition of Co-Pi OECs or adsorption of Co^{2+} ions does not affect the flatband potential of the α-Fe_2O_3 electrodes. This also suggests

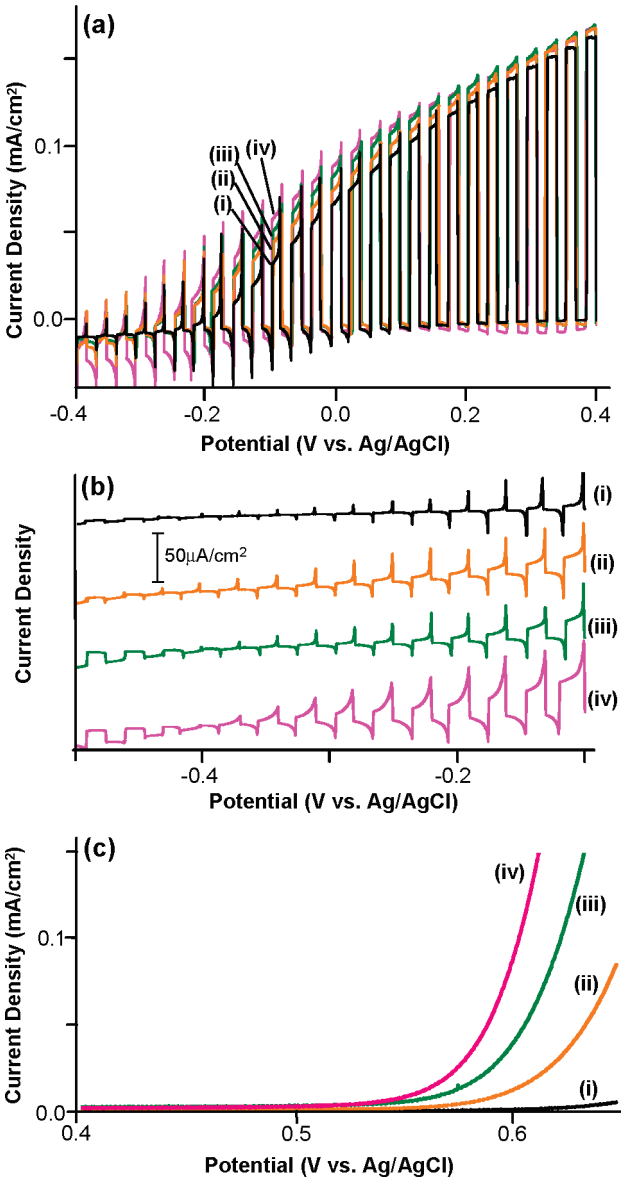

Figure 5. (a) Current−potential characteristics with chopped light and (b) an expanded plot of the same current−potential characteristics near the flatband potential measured in 1 M NaOH (100 mW/cm^2, AM 1.5 illumination). (c) Current−potential characteristics in the dark near the electrochemical onset potential for O_2 evolution. (i) α-Fe_2O_3 (black), (ii) α-Fe_2O_3/adsorbed Co^{2+} (orange), (iii) α-Fe_2O_3/Co-Pi OEC (OC) (green), and (iv) α-Fe_2O_3/Co-Pi OEC (SC) (pink).

that any photocurrent enhancement observed with the α-Fe_2O_3 electrodes containing Co-Pi OEC or adsorbed Co^{2+} ions is solely due to the catalyst's ability to improve water oxidation kinetics and not due to changes in interfacial energetics (e.g., flatband potential, band bending).

Panels a and b in Figure 5 show that all α-Fe_2O_3 electrodes containing Co-Pi OEC or Co^{2+} ions generate more photocurrent than the bare α-Fe_2O_3 electrode, and their effect on photocurrent enhancement increases in the order of Co^{2+} < Co-Pi OEC (OC) < Co-Pi OEC (SC). The effect of these catalysts on O_2 evolution is also evident in the dark scan that shows the onset of electrochemical O_2 evolution shifting to the negative direction (decreasing overpotential) (Figure 5c). The

dx.doi.org/10.1021/cm1020614 |*Chem. Mater.* 2011, 23, 1686–1693

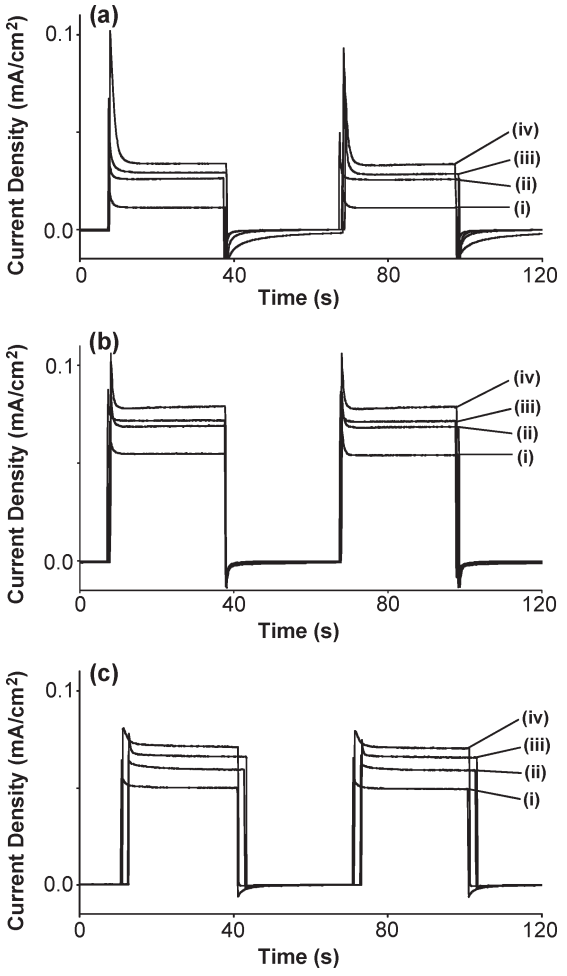

Figure 6. Photocurrents measured while applying a constant potential of (a) −0.1 V and (b) +0.1 V vs Ag/AgCl in 1 M NaOH and (c) +0.1 V vs Ag/AgCl in 1 M NaOH solution containing 0.1 M KH_2PO_4 (100 mW/cm^2, AM 1.5 illumination). (i) α-Fe_2O_3, (ii) α-Fe_2O_3/adsorbed Co^{2+}, (iii) α-Fe_2O_3/Co-Pi OEC (OC), and (iv) α-Fe_2O_3/Co-Pi OEC (SC).

Co-Pi OEC (SC) on the α-Fe_2O_3 electrode resulted in the most significant reduction in overpotential followed by Co-Pi OEC (OC) and then by surface adsorbed Co^{2+} ions, which is exactly the same trend as that observed in photocurrent enhancement. This result shows that nanoparticulate Co-Pi OECs grown under the SC condition with a higher yield and a higher nucleation density can maximize the catalytic ability. Simply increasing deposition time of the Co-Pi OEC using the OC condition resulted in the growth of larger Co-Pi OEC particles that hindered photon absorption by α-Fe_2O_3 and decreased the photocurrent.

To confirm that the photocurrent enhancement observed in the LSV with chopped light is not only for the transient photocurrent but also for steady-state photocurrent, photocurrents were measured while applying a constant bias of −0.1 and 0.1 V vs Ag/AgCl. Figure 6 shows that the same enhancements are observed for the steady state photocurrents. Also, as observed in the LSVs, the photocurrent enhancement caused by the presence of Co-Pi OECs or Co^{2+} ions are more pronounced at a more negative bias near the flatband potential. For example, the photocurrent improvement caused by Co-Pi OEC (SC), Co-Pi OEC(OC), and adsorbed Co^{2+} ions are 3, 2.5, and 2.3 times at −0.1 V and 1.5, 1.3, and 1.2 times at +0.1 V over the

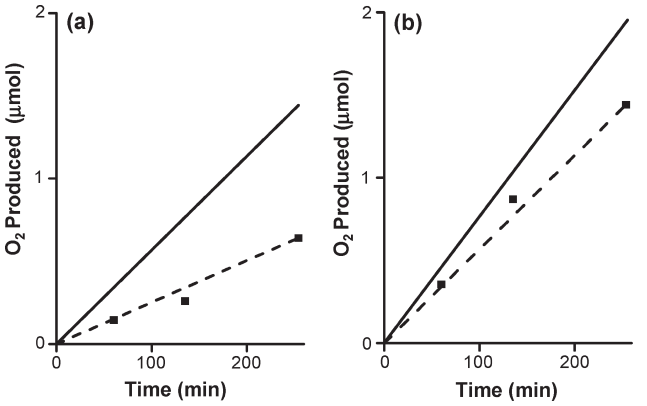

Figure 7. O_2 detected by a fluorescence based sensor (---), and O_2 calculated from photocurrent passed (—) during illumination of (a) a bare α-Fe_2O_3 electrode and (b) a α-Fe_2O_3/Co-Pi OEC (SC) electrode using 1 M NaOH solution containing 0.1 M KH_2PO_4 (light intensity, 600 mW/cm^2; applied bias, +0.2 V vs Ag/AgCl).

photocurrent of the unaltered α-Fe_2O_3 electrode. This result suggests that the Co-Pi OECs can efficiently reduce electron−hole recombination in the low band bending region by improving the interfacial hole transfer and O_2 evolution kinetics.

We also tested the stability of the Co-Pi OECs in 1 M NaOH solution for a prolonged period of illumination (4 h) under a constant bias of +0.2 V vs Ag/AgCl. The SEM image of the resulting electrode shows that while the loading amount of Co-Pi OEC (SC) did not decrease over time, the morphology of the Co-Pi OEC deposits was changed (see the Supporting Information, Figure S4). In addition, the XPS analysis shows that the Co:P ratio was also changed to 1:0.06−0.1. This suggests that the Co-Pi OEC goes through the dissolution and redeposition processes during the catalytic cycle of O_2 production in 1 M NaOH solution as in the case of pH 7 phosphate buffer solution.[18,19] Since the 1 M NaOH solution does not contain phosphates, the Co-Pi OEC loses phosphates over time and changes its composition and morphology. However, when 0.1 M KH_2PO_4 was added to 1 M NaOH, the morphology of the Co-Pi OEC (SC) as well as the Co:P ratio remained unchanged after 4 h of illumination at +0.2 V vs Ag/AgCl (see the Supporting Information, Figure S4). The photocurrents obtained in 1 M NaOH solution containing 0.1 M KH_2PO_4 are shown in Figure 6c, which are comparable to those obtained in 1 M NaOH solution (Figure 6b).

In order to confirm that the photocurrent enhancement achieved by Co-Pi OECs is truly due to the enhancement in O_2 evolution and not by other photo-oxidation reactions (e.g., alteration or charging of the Co-Pi OEC that does not result in O_2 production), we measured the O_2 gas produced by the bare α-Fe_2O_3 and the α-Fe_2O_3/Co-Pi OEC (SC) electrodes using a fluorescence-based O_2 sensor while also recording the photocurrent at +0.2 V vs Ag/AgCl using 1 M NaOH solution containing 0.1 M KH_2PO_4 as the electrolyte. Then the actual amount of detected O_2 was compared with the theoretical amount of O_2, which was calculated from the generated photocurrent by assuming 100% Faradaic efficiency, in order to obtain the photocurrent to O_2 conversion efficiency.

The result shows that the presence of the Co-Pi OEC (SC) on the α-Fe_2O_3 electrode not only increased the total amount of photocurrent generated (i.e., theoretical amount of O_2 calculated

dx.doi.org/10.1021/cm1020614 |*Chem. Mater.* 2011, 23, 1686–1693

from photocurrent) but also increased the photocurrent to O_2 conversion efficiency significantly (Figure 7). (Although ca. 45% of the photocurrent generated by the bare α-Fe_2O_3 electrode was associated with O_2 production, ca. 82% of the photocurrent generated by the α-Fe_2O_3/Co-Pi OEC (SC) electrode was used to produce O_2.) This result clearly confirms that the presence of Co-Pi OECs on the α-Fe_2O_3 electrode facilitates O_2 production kinetics as well as electron−hole pair separation.

CONCLUSIONS

We have prepared α-Fe_2O_3/Co-Pi OEC electrodes to investigate the interaction between the n-type α-Fe_2O_3 electrode and Co-Pi OECs. The α-Fe_2O_3 electrodes were prepared by electrodeposition of nanocrystalline Fe metal films using a nonaqueous medium followed by annealing the film at 500 °C in air. Co-Pi OECs were photochemically deposited onto α-Fe_2O_3 electrodes using both OC and SC conditions. The SC condition, which separates the photo-oxidation reaction from the photoreduction reaction, significantly increased the nucleation density and the amount of Co-Pi OEC deposited. The SC condition also resulted in a lower Co^{2+}/Co^{3+} ratio in the Co-Pi OEC by removing the influence of the photoreduction reaction on the photo-oxidation reaction. Photocurrent measurements show that photodeposited Co-Pi OECs improved the photocurrent of α-Fe_2O_3 electrodes more than Co^{2+} ions simply adsorbed on the α-Fe_2O_3 surface, with the Co-Pi OEC deposited under the SC condition resulting in the most pronounced photocurrent enhancement. This is because the SC condition significantly improves the coverage of the α-Fe_2O_3 surface by Co-Pi OEC nanoparticles with a high nucleation density, which ensures that all the active sites for photo-oxidation are covered by Co-Pi OEC particles but interference of Co-Pi OECs with light absorption by the α-Fe_2O_3 electrode remains minimal. This study demonstrated that creating a SC condition for photodeposition of Co-Pi OEC provides a more efficient way to produce a semiconductor/Co-Pi OEC photoanode system. The long-term stability test shows that while the Co-Pi OEC changes its composition and morphology over time in 1 M NaOH solution, it is stable in 1 M NaOH solution containing 0.1 M KH_2PO_4. The O_2 detection measurements show that the presence of photodeposited Co-Pi OEC on the α-Fe_2O_3 surface not only increases the total amount of photocurrent by facilitating electron−hole pair separation but also increases the photocurrent to O_2 conversion efficiency by improving O_2 evolution kinetics.

ASSOCIATED CONTENT

Supporting Information. UV−vis spectrum and XRD of α-Fe_2O_3 electrode, curve fitting of Co 2p XPS spectra of Co-Pi OECs, and SEM images of the α-Fe_2O_3 /Co-Pi OEC (SC) electrodes after long-term photocurrent measurements. This information is available free of charge via the Internet at http://pubs.acs.org.

AUTHOR INFORMATION

Corresponding Author

*E-mail: kchoi1@purdue.edu. Tel: (765) 494-0049. Fax: (765) 494-0239.

ACKNOWLEDGMENT

This work was financially supported by a Center for Chemical Innovation of the National Science Foundation (Grant CHE-0802907) and made use of the Life Science Microscopy Facility at Purdue University. The XPS data was obtained by Dr. D. Zemlyanov of the Surface Analysis Laboratory, Birck Nanotechnology Center, Purdue University and in part by Dr. R. Haasch of the Frederick Seitz Materials Research Laboratory Central Facilities, University of Illinois at Urbana−Champaign.

REFERENCES

(1) Kennedy, J. H.; Frese, K. W. *J. Electrochem. Soc.* **1978**, *125*, 709–714.
(2) Dare-Edwards, M. P.; Goodenough, J. B.; Hamnett, A.; Trevellick, P. R. *Faraday Trans.* **1983**, *1*, 2027–2041.
(3) Kay, A.; Cesar, I.; Gratzel, M. *J. Am. Chem. Soc.* **2006**, *128*, 15714–15721.
(4) Aroutiounian, V. M.; Arakelyan, V. M.; Shahnazaryan, G. E.; Stepanyan, G. M.; Khachaturyan, E. A.; Wang, H.; Turner, J. A. *Sol. Energy* **2006**, *80*, 1098–1111.
(5) Glasscock, J. A.; Barnes, P. R. F.; Plumb, I. C.; Savvides, N. *J. Phys. Chem. C* **2007**, *111*, 16477–16488.
(6) Jang, J. S.; Lee, J.; Ye, H.; Fan, F. R. F.; Bard, A. J. *J. Phys. Chem. C* **2009**, *113*, 6719–6724.
(7) Aroutiounian, V. M.; Arakelyan, V. M.; Shahnazaryan, G. E.; Hovhannisyan, H. R.; Wang, H.; Turner, J. A. *Sol. Energy* **2007**, *81*, 1369–1376.
(8) Turner, J. E.; Hendewerk, M.; Parmeter, J.; Neiman, D.; Somorjai, G. A. *J. Electrochem. Soc.* **1984**, *131*, 1777–1783.
(9) Kleiman-Shwarsctein, A.; Hu, Y.-S.; Forman, A. J.; Stucky, G. D.; McFarland, E. W. *J. Phys. Chem. C* **2008**, *112*, 15900–15907.
(10) Beermann, N.; Vayssieres, L.; Lindquist, S.-E.; Hagfeldt, A. *J. Electrochecm. Soc.* **2000**, *147*, 2456–2461.
(11) Spray, R. L.; Choi, K. S. *Chem. Mater.* **2009**, *21*, 3701–3709.
(12) Prakasam, H. E.; Varghese, O. K.; Paulose, M.; Mor, G. K.; Grimes, C. A. *Nanotechnology* **2006**, *17*, 4285–4291.
(13) Lindgren, T.; Wang, H.; Beermann, N.; Vayssieres, L.; Hagfeldt, A.; Lindquist, S.-E. *Sol. Energ. Mat. Sol. C* **2002**, *71*, 231–243.
(14) LaTempa, T. J.; Feng, X. J.; Paulose, M.; Grimes, C. A. *J. Phys. Chem. C* **2009**, *113*, 16293–16298.
(15) Kleiman-Shwarsctein, A.; Hu, Y. S.; Stucky, G. D.; McFarland, E. W. *Electrochem. Commun.* **2009**, *11*, 1150–1153.
(16) Zhong, D. K.; Sun, J. W.; Inumaru, H.; Gamelin, D. R. *J. Am. Chem. Soc.* **2009**, *131*, 6086–6087.
(17) Zhong, D. K.; Gamelin, D. R. *J. Am. Chem. Soc.* **2010**, *132*, 4202–4207.
(18) Kanan, M. W.; Nocera, D. G. *Science* **2008**, *321*, 1072–1075.
(19) Kanan, M. W.; Surendranath, Y.; Nocera, D. G. *Chem. Soc. Rev.* **2009**, *38*, 109–114.
(20) Lutterman, D. A.; Surendranath, Y.; Nocera, D. G. *J. Am. Chem. Soc.* **2009**, *131*, 3838–3839.
(21) Surendranath, Y.; Dinca, M.; Nocera, D. G. *J. Am. Chem. Soc.* **2009**, *131*, 2615–2620.
(22) Kanan, M. W.; Yano, J.; Surendranath, Y.; Dinca, M.; Yachandra, V. K.; Nocera, D. G. *J. Am. Chem. Soc.* **2010**, *132*, 13692–13701.
(23) Steinmiller, E. M. P.; Choi, K. S. *Proc. Natl. Acad. Sci. U.S.A.* **2009**, *106*, 20633–20636.
(24) Pourbaix, M. *Atlas of Electrochemical Equilibria in Aqueous Solutions*, 2nd English ed.; National Association of Corrosion Engineers: Houston, TX, 1974.
(25) Diaz, S. L.; Calderon, J. A.; Barcia, O. E.; Mattos, O. R. *Electrochim. Acta* **2008**, *53*, 7426–7435.
(26) Abd el Meguid, E. A.; Abe el Rehim, S. S.; Moustafa, E. M. *Thin Solid Films* **2003**, *443*, 53–59.
(27) Yoshimura, S.; Yoshihara, S.; Shirakashi, T.; Sato, E. *Electrochim. Acta* **1994**, *39*, 589–595.

(28) Kim, K. H.; Lee, J. D.; Lee, J. J.; Ahn, B. Y.; Kim, H. S.; Shin, Y. W. *Thin Solid Films* **2005**, *483*, 74–78.
(29) Allen, G. C.; Hallam, K. R. *Appl. Surf. Sic.* **1996**, *93*, 25–30.
(30) Wagner, C. D.; Riggs, W. M.; Davis, L. E.; Moulder, J. F.; Muilenberg, G. E., Eds. *Handbook of X-Ray Photoelectron Spectroscopy: A Reference Book of Standard Data for Use in X-ray Photoelectron Spectroscopy*; Perkin-Elmer: Eden Prairie, MN, 1979.
(31) Foelske, A.; Strehblow, H. H. *Surf. Interface Anal.* **2002**, *34*, 125–129.
(32) Foelske, A.; Strehblow, H. H. *Surf. Interface Anal.* **2000**, *29*, 548–555.
(33) Foelske, A.; Kunze, J.; Strehblow, H.-H. *Surf. Sci.* **2004**, *554*, 10–24.
(34) McAlpin, J. G.; Surendranath, Y.; Dinca, M.; Stich, T. A.; Stoian, S. A.; Casey, W. H.; Nocera, D. G.; Britt, R. D. *J. Am. Chem. Soc.* **2010**, *132*, 6882–6883.
(35) Tan, B. J.; Klabunde, K. J.; Sherwood, P. M. A. *J. Am. Chem. Soc.* **1991**, *113*, 855–861.
(36) Hardee, K. L.; Bard, A. J. *J. Electrochem. Soc.* **1977**, *124*, 215–224.
(37) Fredlein, R. A.; Bard, A. J. *J. Electrochem. Soc.* **1979**, *126*, 1892–1898.
(38) Risch, M.; Khare, V.; Zaharieva, I.; Gerencser, L.; Chernev, P.; Dau, H. *J. Am. Chem. Soc.* **2009**, *131*, 6936–6937.